



A big landslide on the Jinsha River, Tibet, China: geometric characteristics, causes, and future stability

Yulong Cui¹ · Pengpeng Bao¹ · Chong Xu² · Gui Fu¹ · Qisong Jiao² · Yi Luo² · Lingling Shen³ · Xiwei Xu² · Fenglin Liu² · Yuejun Lyu² · Xiuhong Hu² · Tao Li² · Yongsheng Li² · Yimin Liu² · Yunfeng Tian²

Received: 21 December 2019 / Accepted: 24 August 2020 / Published online: 1 September 2020
© Springer Nature B.V. 2020

Abstract

On October 10, 2018, a big landslide occurred on the right bank of the Jinsha River in Baige Village, Polo Township, Jiangda County, Tibet (hereafter called the Baige landslide), which blocked the Jinsha River, forming a barrier lake. Afterward, the landslide dam broke, producing a flood. On November 3, the rear wall of this landslide failed again, also blocking the Jinsha River and creating a bigger barrier lake. Then, by local people, a discharge channel was excavated on the top of the landslide dam, making lake water cross over the discharge channel. As the water flow gradually increased, the landslide dam broke again, producing a more severe flood, resulting in huge economic losses downstream. The purpose of this study is to understand the cause of this landslide and predict the future stability of its head scarp, providing some support for the control scheme in the later stage. A digital orthophoto map (DOM) and a digital elevation model (DEM) of the landslide were created using an unmanned aerial vehicle. Then based on the DOM and DEM, the geometric characteristics of the landslide were described. Multi-phase Planet 5 images were used to infer the development process of the landslide. Finally, the cause of the landslide was analyzed based on the rainfall data and the limit equilibrium calculation. The results show that the Baige landslide was a self-weight creeping event, and its development and trigger were independent of the rainfall. Before the landslide, the slope experienced five stages of evolution: steady deformation, slow deformation, rapid deformation, steady deformation, and rapid deformation. The limit equilibrium calculation indicates that the stability coefficient of the middle section of the head scarp is the lowest, thus which should be cut down as a priority. This study provides a typical example of a self-weight creep type landslide, and an important reference for prediction and prevention of similar large landslides in the Tibetan Plateau, southwestern China.

✉ Chong Xu
xc11111111@126.com; xuchong@ies.ac.cn

¹ School of Civil Engineering and Architecture, Anhui University of Science and Technology, Huainan 232001, China

² National Institute of Natural Hazards, Ministry of Emergency Management of China (Former Institute of Crustal Dynamics, China Earthquake Administration), Beijing 100085, China

³ Beijing Meteorological Information Center, Beijing Meteorological Service, Beijing 100089, China

Keywords Baige landslide · Geometric characteristics · Cause · Stability · Tibetan plateau

1 Introduction

At 22:05 on October 10, 2018, a landslide occurred at Baige Village, Polo Township, Jianga County, Tibet (E98°42'18", N31°4'57") (Zhang et al. 2019b). It is on the right bank of the Jinsha River, and deposits of its toe blocked the river to form a barrier lake. By 0:45 on October 13, the lake storage reached $2.9 \times 10^8 \text{ m}^3$, then the water flew over the top leading to a flood. All the lake water drained out on that day. At 17:40 on November 3, the head scarp of the landslide failed and slid down, blocking the Jinsha River again, creating a larger barrier lake. On November 12, the lake storage reached $5.24 \times 10^8 \text{ m}^3$. Soon after, by local people, a drainage sump was excavated on the dam to allow the lake water to flow out. The next day, the upstream and downstream water levels of the dam were at the same height, and the danger was mitigated (Deng et al. 2019; Wu et al. 2019; Zhang et al. 2019a, b). Due to the proper countermeasures taken by the government, this event did not cause any casualties. However, a large amount of infrastructure and farmland were destroyed by the barrier lake and the two discharge floods. The economic loss to Yunnan Province amounted to 7 billion RMB.

China is one of the countries with the most serious landslide disasters in the world (Xu et al. 2014, 2015). The annual economic losses caused by landslide disasters are more than 20 billion RMB in addition to a large number of casualties. Examples of recent years are as follows. On August 11, 2019, the typhoon Lekima caused many geological disasters including landslides and debris flows. Among them, a landslide and its dammed lake killed 32 people in Shanzao Village, Yantan Town, Yongjia County, Zhejiang Province. On July 23, 2019, a huge landslide caused by heavy rainfall in Jichang Town, Shuicheng County, Liupanshui City, Guizhou Province killed 33 people, with 18 people missing, and 11 people injured. On March 15, 2019, in Zaoling Township, Xiangning County, Linfen City, Shanxi Province, a loess landslide of an area of 10^5 m^2 killed 20 people (Cui et al. 2020; Ma et al. 2020). On August 28, 2017, a landslide in Zhangjiawan, Nayong County, Guizhou Province, killed 26 people, 9 people missing, and 8 people injured (Fan et al. 2019a; Zhu et al. 2019). On September 28, 2016, a landslide in Sucun, Suichang County, Zhejiang Province, killed 27 people (Ouyang et al. 2019). And on July 18, 2010, a landslide caused by heavy rainfall in Qiyan Village, Ankang City, Shaanxi Province killed 29 people (Fan et al. 2019b).

In the western mountainous areas of China, the history documented several landslide and barrier lake disasters with heavy casualties. For example, in 1786, a landslide triggered by the M 7.75 earthquake in the Kangding-Luding region of Sichuan Province blocked the Dadu River, and then the dam burst and the flood killed 100,000 people downstream (Dai et al. 2005; Evans et al. 2011). In 1933, an M 7.5 earthquake occurred in Dixi Town, Sichuan Province, which created three continuous landslide dams on the Min River, afterward the last dam on the downstream side burst and the resulting flood causing 2,500 deaths (Chai et al. 2000; Wang et al. 2011). In 1917, an M 6.7 earthquake occurred in the Beiguan River basin in Yunnan Province, which formed a barrier lake where more than 1600 people were drowned (Chai et al. 1995). In summary, throughout history, in almost every month, several landslides have caused dozens of deaths in China.

With rapid economic growth and development of science and technology, the Chinese government has put tremendous resources into investigation, evaluation, monitoring, early

warning, control, and emergency response of landslides. These efforts have achieved some results; some landslides have been successfully predicted and dealt with. For example, on July 19, 2018, a landslide in Taozi town, Yanyuan City, Sichuan Province, was successfully predicted, and hundreds of deaths were prevented due to the emergent implementation of preventative methods (Hu et al. 2019). On May 5, 2018, a landslide occurred in Mabian County, Sichuan Province. No casualties were caused by this event due to forecast ahead and the emergent traffic control implemented (Ma et al. 2018; Wei et al. 2019). On March 12, 2019, Chang'an University and the Chengdu University of Technology successfully predicted two loess landslides in Heifangtai, Yongjing County, Gansu Province, and possible casualties were avoided. However, due to China's vast area, complex geography, geomorphology, geological conditions and complex landslide mechanisms, landslide disaster prevention remains a challenging issue, especially in the Tibetan Plateau and the Loess Plateau in western mainland.

The occurrence of landslides is controlled by the nature of the slope itself including the slope structure, lithology, and the slope landform as well as external inducing factors including earthquakes, rainfall, groundwater, and human activities (Varnes 1958). The external inducing factors of most landslides in China in recent years fall into the above categories. However, no major earthquakes were recorded in the vicinity of the Baige landslide for many years prior to the landslide, nor was the area affected by strong earthquake waves from a distance. Data available show that there were no obvious rainfall events or nearby human activity before the landslide. Thus, the cause of the Baige landslide remains to be clarified.

In this study, we create a digital orthophoto map (DOM) and a digital elevation model (DEM) for the Baige landslide using an unmanned aerial vehicle (UAV). Based on the DOM and DEM, the geometric characteristics of the landslide are described. Multi-period Planet 5 historical images are used to analyze the development process of the landslide. The causes of the landslide are interpreted based on the rainfall data and the limit equilibrium calculation. Finally, the future stability of the head scarp of the landslide is predicted, and several correction recommendations are given.

2 Geomorphic and geological setting

The Baige landslide is located on the southeastern margin of the Tibetan Plateau, a transitional slope zone from the Tibetan Plateau and the Yunnan-Guizhou Plateau to the Sichuan Basin. The Jinsha River flows from north to south through this region, where mountains are deeply incised. The bedrock slope above the river bed at an elevation of 100 m is greater than 60°. A narrow valley about 100–200 m wide and a wide valley about 200–400 m wide coexist in this region (Fig. 1). The landslide area hosts alpine and canyon landforms with significant topographic relief. The lowest elevation is 2800 m, and the highest is 5436 m, about 3800 m on average, and the maximum height difference is 2636 m. The climate of the landslide area is subtropical. The precipitation at the Baiyu meteorological station on the west side of the Jinsha River is only 365 mm from July to September every year. The annual average temperature is about 15 °C, with the highest temperature 35 °C. This region is a subtropical arid valley.

Many strata are exposed in the landslide area, including Ordovician, Carboniferous, Permian, Triassic, and Jurassic, with allochthonous terranes at some places. The lower part of the Baige landslide is Jurassic monzonitic granite, and the upper part is

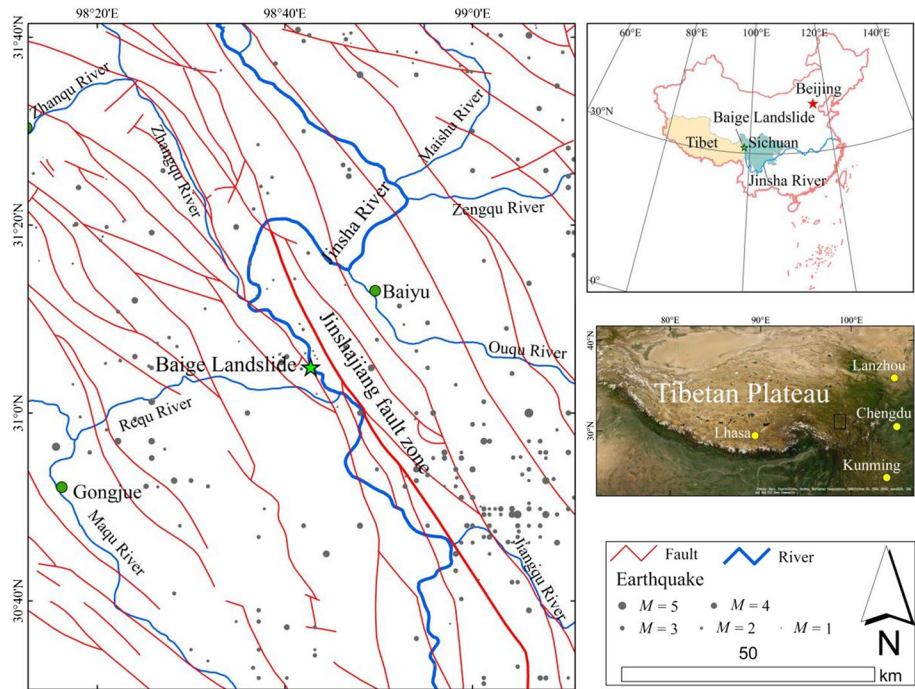


Fig. 1 Tectonic setting (left) and geographical location (right) of the study area. The earthquakes since 1900 are from the China Earthquake Data Center (<https://data.earthquake.cn>). The faults are from Deng (2007) and Xu et al. (2016)

the Permian Ningduo Group, with gneiss and quartz schist. Faults developed well in the landslide area, and a fault crosses through the back part of the landslide. The landslide is located on the western side of the Jinshajiang fault zone, a complex tectonic zone trending southeast, about 700 km long and 80 km wide. It consists of 6–7 trunk faults, most of which are median-angle thrusts with right-lateral slip. The Jinshajiang fault zone is now shortening at an annual rate of 2–3 mm/yr in a nearly EW direction (Zhou et al. 2005). A large number of giant ancient landslides and lake deposits have been identified downstream of the Baige landslide at the intersection of the Jinsha River and the Jinshajiang fault zone, or the reach nearest the fault zone. These landslides were considered to be triggered by earthquakes in 122–1100 AD (Chen et al. 2013, 2018), likely M 7.0–7.4 (Long et al. 2015). Since 1900, 288 earthquakes took place in the landslide area, including 282 M 0–4.0, 6 greater than M 4.0, with the maximum M 5.1 (Fig. 1).

Fifty-five ancient landslides were identified in a 45×50 km area centered at the landslide, while a little in a larger region (Fig. 2). Exceptionally, on the right bank of the Jinsha River near the Baige landslide, ancient landslides are densely distributed, where within an area of 7180×10^4 m² 17 ancient landslides have been recognized, with a total area of 1010×10^4 m², accounting for 14.1% of the entire area. The largest individual landslide reaches 198×10^4 m² (Fig. 2).

According to the geological map (Fig. 2), the landslide was crossed by a reverse fault. The upper part of the landslide, that is, the hanging wall of the fault, is the T₂₋₃d-dk

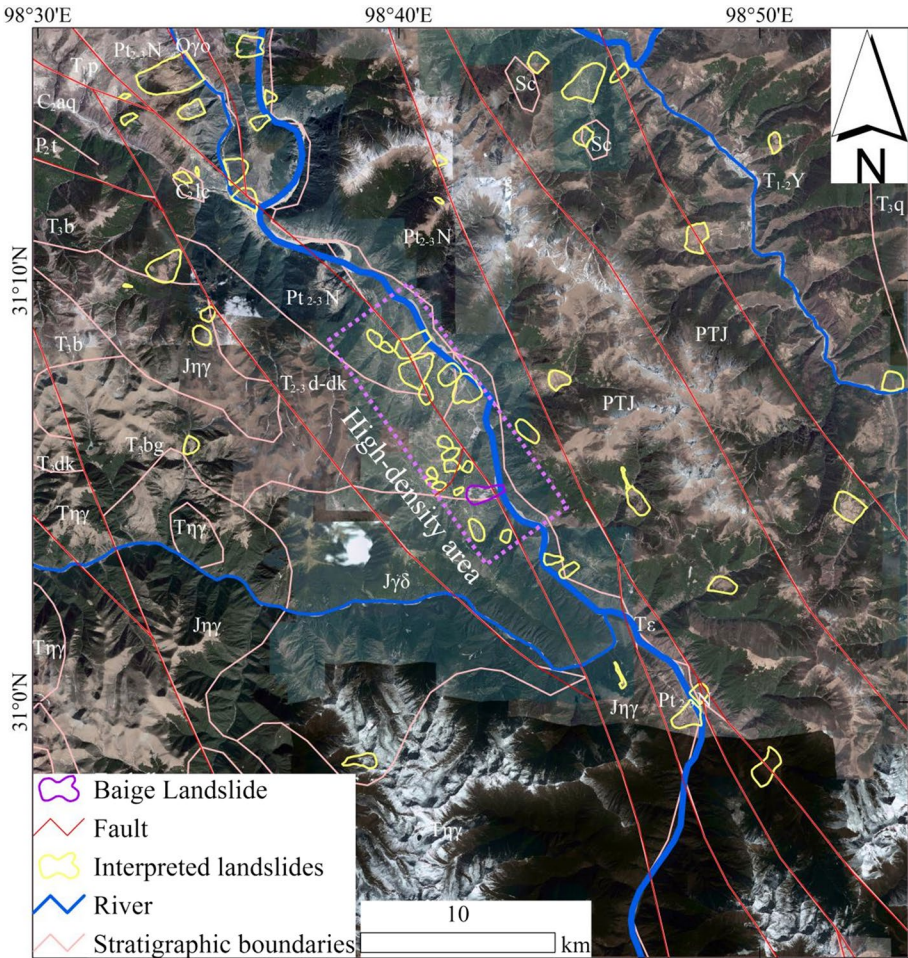


Fig. 2 Geology and ancient landslides in the study area. The geologic data are from China Geological Survey (<https://www.ngac.org.cn>). Triassic: T_ε, T_{1,2Y}, T_{1p}, T_{2,3d-dk}, T_{3bg}, T_{3b}, T_{3dk}, T_{3g}, T_{3q}, T_{γδ}, T_{δu}, T_{ηγ}; Carboniferous: C_{2aq}, C_{2lc}; Jurassic: J_{γδ}, J_{ηγ}; Ordovician: O_{γo}; Permian: PTJ., PTJ, Pt_{2,3 N}, P₂; Allochthonous Terrane: Sc

stratum, and the lithology is gneiss and greenschist. The lower part of the landslide, that is, the foot wall of the fault, is Jηγ stratum, and the lithology is granite.

3 Data and methods

This work built on analysis of images, geomorphology, rainfall, and a limit equilibrium calculation, as described below.

The data used in this study are as follows: Free download 3 m resolution Planet 5 images; A DOM with 0.2 m resolution and a DEM with 0.14 m resolution of the Baige landslide shoot by the DJ Pro4 UAV; Free download ALOS 12.5 m resolution DEM, the

rainfall data from 2010 to 2017 from the Baiyu meteorological station. All the projection coordinates of the images and DEM are WGS_84_UTM_zone_47N. Because the sources of these images and DEM are not consistent, the DOM and DEM shoot by the UAV were then selected as the basis for calibration. First, some marker points were selected, and then the geographic registration of the images and DEM were carried out by the artificial visual method.

The research methods are as follows: (1) The elevation of the exiting shear surface of the landslide front was estimated according to the images taken before the landslide. (2) The contours before the landslide, after the first landsliding, and after the second landsliding were manually drawn. These topographies were used to analyze the geometric characteristics of the landslide, to estimate the volume, and to carry out the limit equilibrium calculation. (3) 12 sets of Planet 5 images from December 2009 to September 2018 were taken to infer the deformation evolution process before the landslide occurrence. The cause of the landslide was analyzed based on the rainfall data from the Baiyu Meteorological Station near the landslide and other data such as seismicity and human activity. (4) According to the limit equilibrium principle (Yang et al. 2015; Zhou and Cheng 2014), the stability was calculated using the Morgenstern-Price method (Morgenstern and Price 1965) and the GeoStudio 2007. Then the cause of the landslide was further analyzed, and the future stability of the back and side-walls of the landslide was predicted.

4 Results

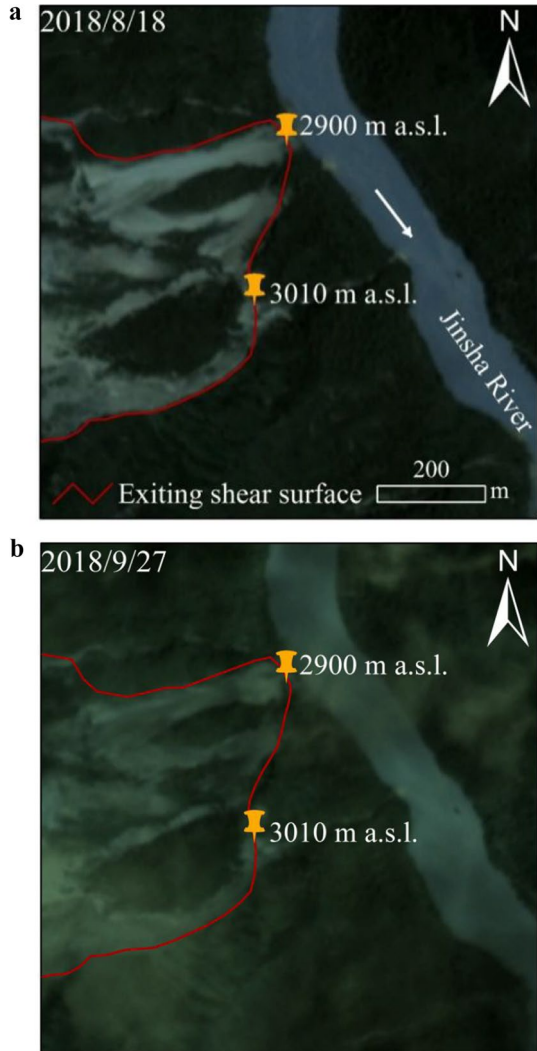
4.1 The geometry of Baige Landslide

After the landsliding, most of the sliding material accumulated in the Jinsha River valley, covering the toe of the landslide source area, thus difficult to identify the exiting shear surface. This problem was solved using two sets of Planet 5 images taken before the landslide on August 18 and on September 27, 2018 (Fig. 3). As shown in Fig. 3, the shape of the exiting shear surface is irregular, the left side is low with an elevation of 2900 m, which is 5 m higher than the water surface of the Jinsha River, and the right side is higher with an elevation of 3010 m.

Using the Planet 5 images taken after the first landsliding on October 17, 2018, the boundary of the source area and the accumulation areas were delineated (Fig. 4a). The upper boundary of the source area is clear on the images, and the lower boundary is the exiting shear surface determined in Fig. 3. Although the middle part of the landslide deposit has been eroded since its deposition, the boundaries on either bank of the Jinsha River are still visible, so the upper and lower boundaries can be estimated. At present, the barrier lake is still visible (Fig. 4a). Although the color at the edges of the accumulation area is significantly different from the region outside the landslide, this section is not composed of landslide deposits, instead of the surge and air impacted area generated during the slide. Three areas of the first landsliding can be determined from the image analysis (Fig. 4). The projected area was measured using the ArcGIS, yielding the source area 712,900 m², the accumulation area 589,200 m², and the surge and air impacted area 476,500 m², respectively.

The geometry of the source area and accumulation area of the second landslide was analyzed using the Planet images taken after the second landsliding on November 9, 2018 (Fig. 4b). The source area of this landslide is located on the head scarp, on the left

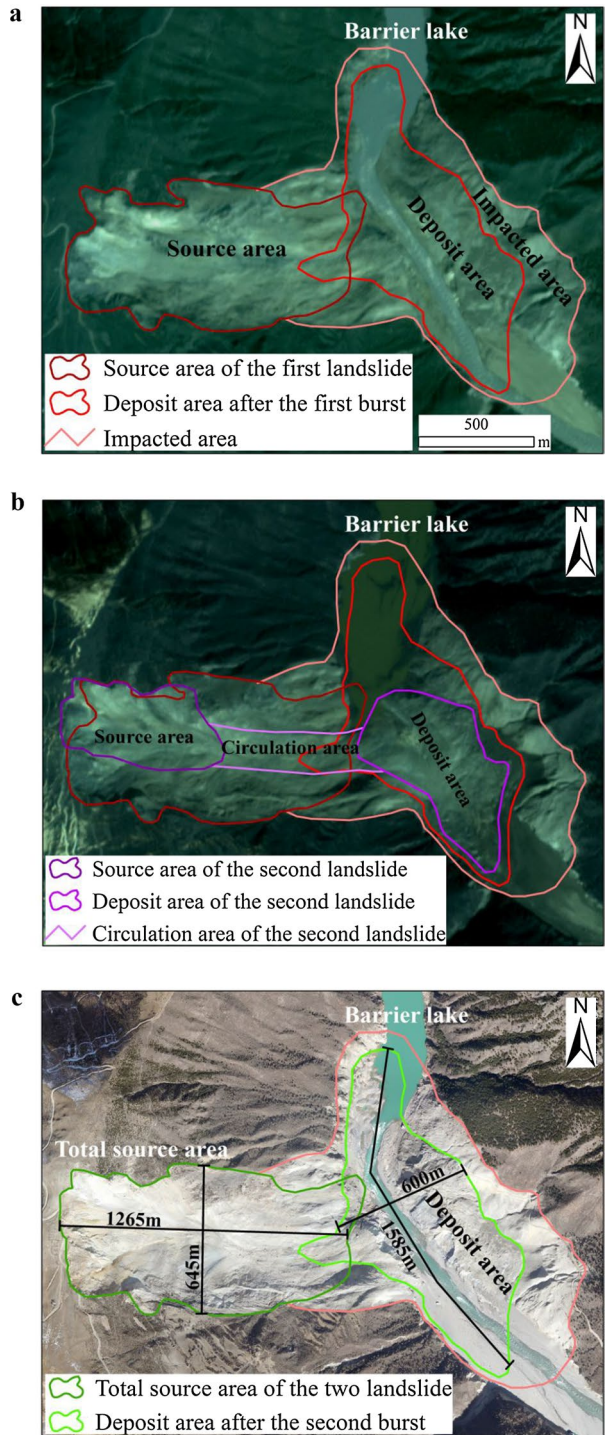
Fig. 3 Leading-edge of the Baige Landslide on the Planet 5 images. **a** Taken on August 18, 2018; **b** Taken on September 27, 2018



side-wall of the first slope failure. The landslide debris passed through the valley's bottom in the source area of the first landslide, accumulated in the eroded channel of the first landslide accumulation area, and blocked the Jinsha River again, forming a new barrier lake. The projected area was measured using the ArcGIS, yielding a source area of 209,100 m² and an accumulation area of 275,300 m², respectively.

The overall geometric characteristics of the two landslides were analyzed using the DOM created using the UAV after the second landsliding. At present, the dam body formed by the second landslide has been broken, as shown in Fig. 4c, which clearly displays the source area, the accumulation area, and the surge and air impacted area of the two landslides. The total source area is the sum of the two landslides, and the total accumulation area and the surge and air impacted area are the same as those of the first landslide. The total source area is roughly rectangular in shape, with a length of 1265 m and a width of 645 m. The leading edge is slightly narrower, and the middle part is slightly wider. The

Fig. 4 Landslide images taken during different periods. **a** Planet 5 images taken on October 17 after the first landslide had occurred, and the dam had broken. **b** Planet 5 images taken on November 9 after the second landslide had occurred, but before the dam broke. **c** The DOM for December 6 after the second landslide had occurred, and the dam had broken



landslide deposits are distributed along the Jinsha River, with a length of 1585 m and a width of 600 m, relatively narrower at the two ends.

Figure 5a shows the terrain obtained using the UAV on December 6 after the second landsliding. The base map is an image overlay of the DEM, and the hill shading was transformed from the DEM in the ArcGIS. The contours with 50-m-interval were generated from the DEM, and its corresponding DOM is shown in Fig. 4c. Four cross-sections were constructed to estimate the thickness of the landslide. Based on the DEM shown in Fig. 4a, contours with 20-m-interval were generated for the source area. Then, the internal contours for the second landslide source area were removed (Fig. 5b). For the micro-topography shown in Fig. 4b, contours with 20-m-interval were manually drawn in the source area before the second landsliding (Fig. 5b). Based on the micro-geomorphology after the first landsliding (Fig. 4a), the contours with 20-m-interval were manually drawn in the accumulation area before the second landsliding (Fig. 5b). The base map in Fig. 5b is an image overlay of the DEM, and the hill shading was generated from the restored contours.

The 20-m-interval contours were generated from the DEM in Fig. 4a, and then the inner contours in the entire source area and accumulation area of the two landsliding in Fig. 4c were removed (Fig. 5c). Based on the micro-geomorphology shown in the Planet 5 image and the ALOS 12.5 m resolution DEM before the two landslides, contours were manually drawn in this area before the two landslides. The generated DEM with the contours and a converted hill-shading were overlain as the base map (Fig. 5c).

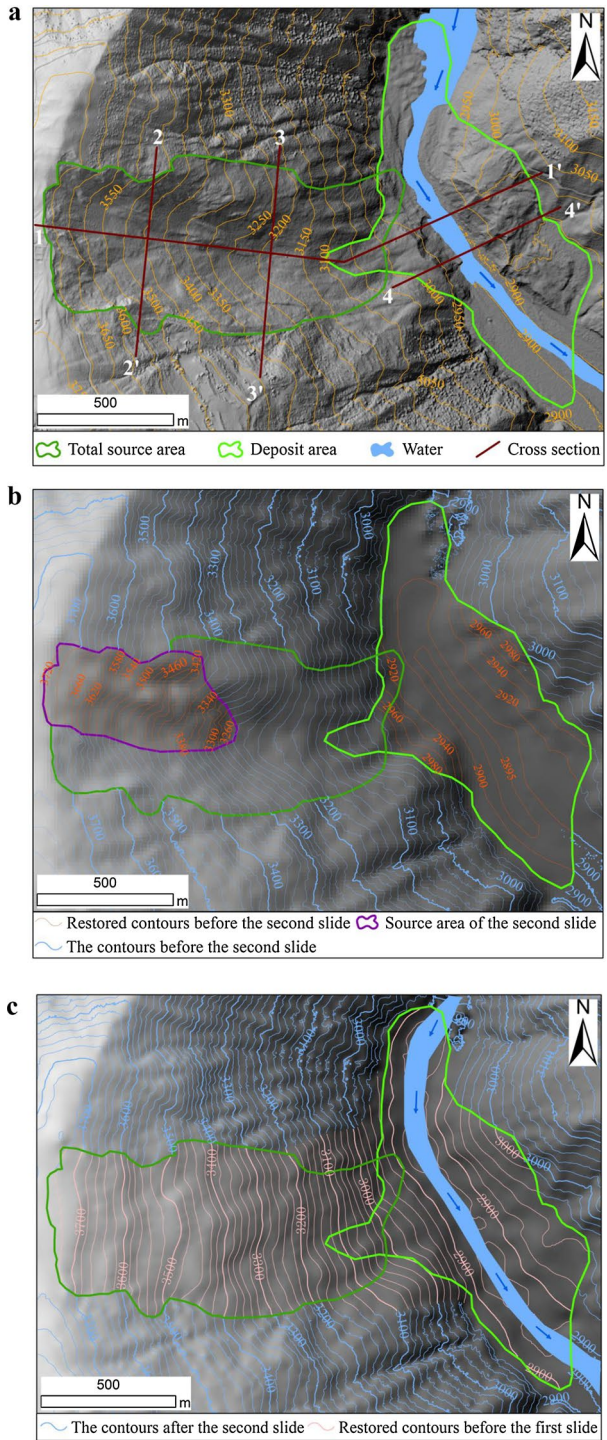
In order to obtain the thickness characteristics of the landslide, a longitudinal section (1–1') passing through the source area and the accumulation area was constructed at the center of the landslide, two cross-sections (2–2' and 3–3') were constructed in the source area, and a cross-section (4–4') perpendicular to the Jinsha River was constructed in the accumulation area (Fig. 5a). As shown in section 1–1', the highest point on the head scarp is 3723 m, the highest point on the landslide deposits is 3105 m, and the elevation of the leading edge is 2981 m (Fig. 6a). The central part of the landslide's source area has a maximum thickness of 140–145 m, while the leading edge has the minimum thickness. The central part of the accumulation area has a maximum thickness of 85–90 m. In section 1–1', the area of the landslide's source is 101,200 m², the area of the accumulation body is 35,800 m², and the area of the eroded area is 17,300 m². The area of overlap between the source area and the accumulation area is 1400 m².

In cross-section 2–2', the area of the landslide's source is 29,600 m², and the slide body is a circular arc with a maximum thickness of 90–95 m (Fig. 6b). Cross-section 3–3' indicates the area of the landslide's source is 22,000 m², and the slide body is approximately trapezoidal with a maximum thickness of 85–90 m (Fig. 6c). The two sides of the trapezoid are two joint faces, the viewing angle of the left joint is 23°, and that of the right joint is 45°. From cross-section 4–4', the maximum thickness of the accumulation body is located at the center of the river valley, with a thickness of 95–100 m and the area of the eroded deposit is 14,600 m² (Fig. 6d).

4.2 The volume of Baige Landslide

Because the deposits of the two landslides were completely washed away and the terrain before the erosion was not recorded, it is difficult to calculate the volumes of the landslides based on the terrain of the deposits. However, the landslide's source is not affected by erosion, so the landslide's volume can be measured and calculated from the terrain of the landslide's source. First, the total volumes of the two landslides were

Fig. 5 Landform in different periods. **a** After the second landsliding and the dam had broken. **b** After the first landsliding and the dam had broken. **c** Before the first landsliding



calculated. The total projected area of the landslide's source area is 685,900 m², while that of the overlapping area is 39,050 m². This only accounts for 5.7% of the source area (Fig. 7a). In addition, the deposits are thin in the overlapping area, so the volume is significantly smaller. Therefore, when calculating the volume, the overlapping area was neglected at first. Except for the overlapping area, the post-sliding DEM was subtracted from the pre-sliding DEM in the source area (Fig. 5a, c), and then the thickness grid was obtained (Fig. 7a). This reveals that the maximum thickness in the source area is 151 m, and its volume was calculated to be 3044×10^4 m³ using the ArcGIS. The volume of the overlapping area is estimated to be 56×10^4 m³, and the total volume of the two landslides is about 3100×10^4 m³.

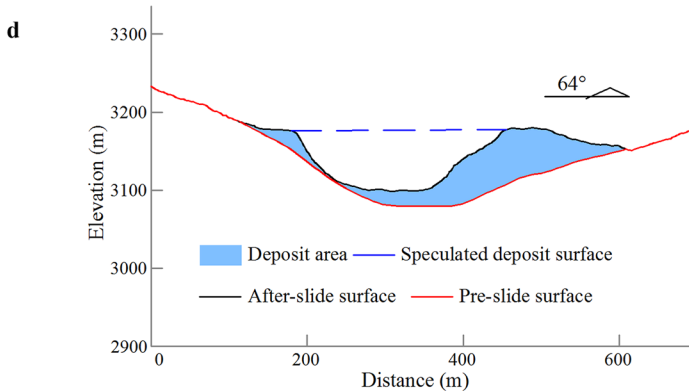
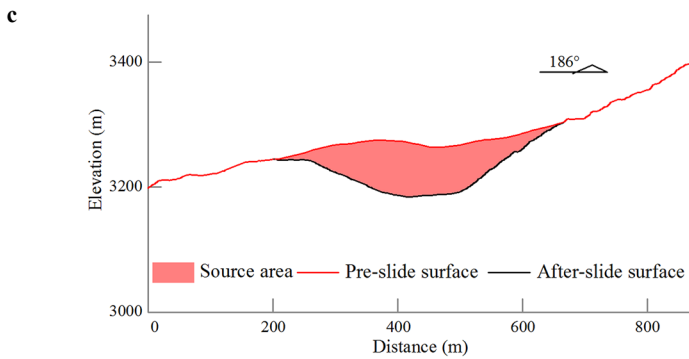
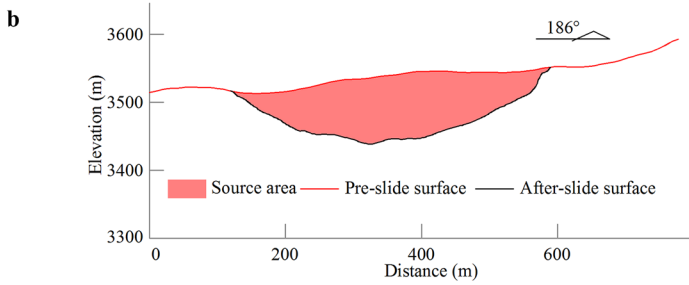
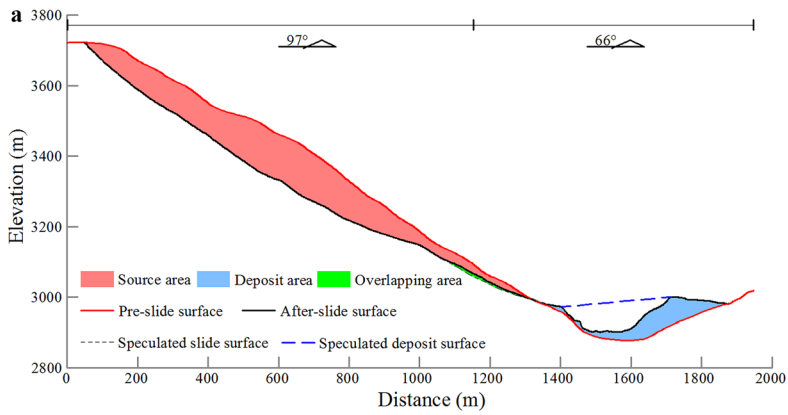
By subtracting the post-sliding DEM from the pre-sliding DEM in the source area of the second landslide (Fig. 5a, b), a thickness grid was produced (Fig. 7b), which reveals that the maximum thickness is 56 m, and its volume was calculated to be 46×10^4 m³ using the ArcGIS. So far, the volumes of the first and second landslides are calculated as 2754×10^4 m³ and 346×10^4 m³, respectively.

4.3 Deformation process of the Baige landslide

Three markers on the image, taken on December 4, 2009, were selected and their positions at different times were interpreted using the ArcGIS. Marker 1 is a country road located in the middle and posterior part of the landslide. Marker 2 is another country road located on the right and back-side of the landslide. And marker 3 is a green vegetation area located at the front of the landslide (Fig. 8). In order to study the evolution process of this landslide, 12 sets of Planet 5 images taken before the landslide between December 4, 2009 and September 24, 2018, were interpreted (Fig. 9). The surface deformation areas on each image were circled one by one with yellow dotted lines.

The total area of the surface deformation area on the images taken on different dates was calculated using the ArcGIS, and the results were mapped (Fig. 10a). It is inferred that the landslide experienced considerable deformation before December 4, 2009, and the surface deformation area reached 117,319 m². From December 2009 to December 2014, the surface deformation area was largely stable. Afterward, the surface deformation area generally increased until September 2018, and the increase was a litter faster. The maximum value was 406,675 m², almost covering the entire landslide.

Taking the positions of the three markers on December 4, 2009, as reference points, their positions in the subsequent images were interpreted using the ArcGIS. The cumulative displacements were measured and plotted (Fig. 10b). It shows that the slope experienced a long period of creep deformation before the Baige landslide. From December 2009 to September 2018, the deformations of markers 1, 2, and 3 reached 78.8 m, 62.2 m, and 57.2 m, respectively. Since December 2009, the creep deformation process of the slope can be divided into five stages: (i) Stage I, from December 2009 to November 2013, steady deformation; (ii) Stage II, from November 2013 to November 2015, slow deformation; (iii) Stage III, from November 2015 to November 2016, intense deformation; (iv) Stage IV, from November 2015 to November 2016, steady deformation; and (v) Stage V, from November 2015 to September 2018, intense deformation. After these five stages of creep deformation, the successive Baige landslides occurred.



◀ **Fig. 6** Four cross-sections of the Baige landslide. **a** Cross-section 1–1'. **b** Cross-section 2–2'. **c** Cross-section 3–3'. **d** Cross-section 4–4'. See Fig. 4a for the locations of these cross-sections

Fig. 7 Thickness grids of the slide body in the source area. **a** The thickness grids for the total of the two slides. **b** The thickness grid for the second slide

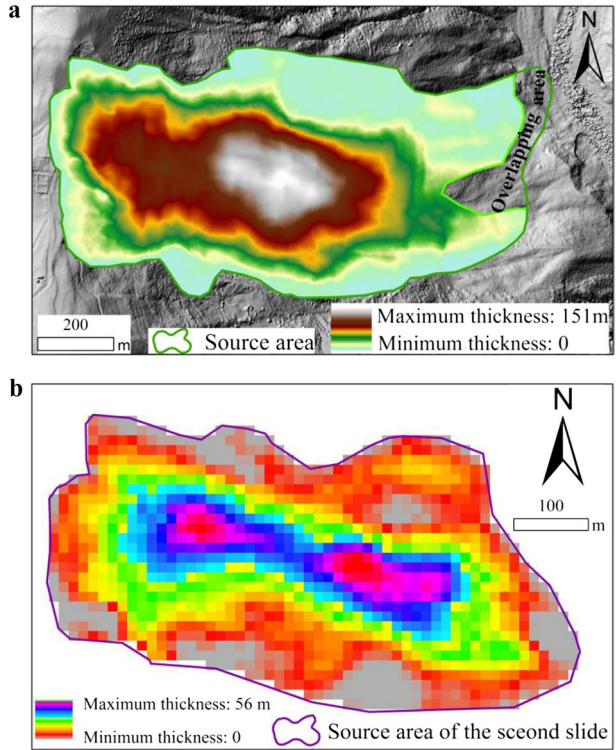
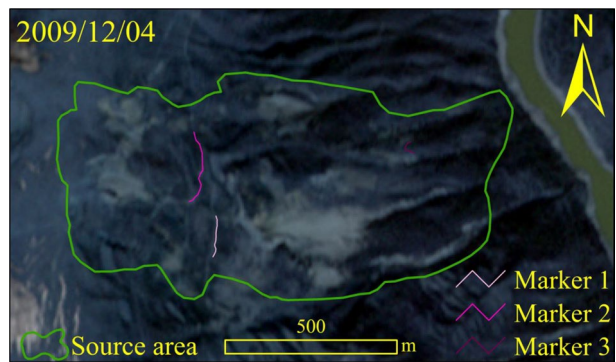


Fig. 8 Three markers on the Planet 5 images of December 4th 2009



4.4 Cause of the Baige landslide

Based on the rainfall data from 2010 to 2017 from the Baiyu meteorological station, which is closest to the landslide with geographic coordinates of N31°13'12", E98°4'48", the relationships between the monthly average rainfall and the cumulative displacements of the

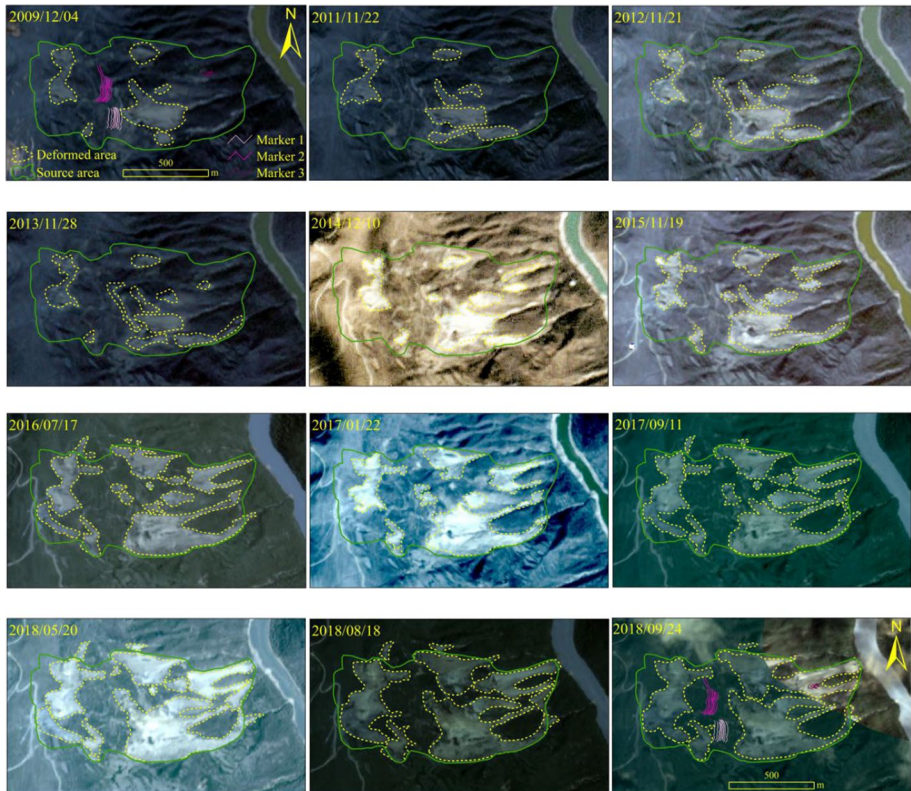


Fig. 9 Sequence of Planet 5 images of the Baige Landslide

three markers were analyzed (Fig. 11). It is clear that the deformation of the landslide is not correlated with the rainfall, i.e., the creep deformation of the landslide was not affected by the rainfall. Combined with the previous analysis, we suggest that the slope experienced creep deformation before 2009 under the action of its self-weight, and the slope deformation was not affected by rainfall. Accompanied by the creep deformation of the slope, the potential slip zone has experienced shear deformation and its strength gradually decreased. When it reached a critically low value, the landslide occurred.

The main longitudinal section (Fig. 6a) was selected for calculation. The calculation model is shown in Fig. 12a. The stability coefficient was calculated by the GeoStudio 2007 using the Morgenstern-Price method. According to the limit equilibrium principle, a stability coefficient of 1 means that the slope is in a limit equilibrium state, and a coefficient less than 1 means that the slope is about to slide. The sliding body-weight γ was assumed as 20 g/cm^3 . The first set of calculation parameters included a cohesion c of 35 kPa, an internal friction angle φ of 40° , and the other calculation parameters gradually decreased (Table 1). The calculation results of the stability factors shown in Table 1 are plotted in Fig. 12b, indicating that as the strength parameters of the sliding zone decrease, the stability coefficient gradually decreases. When the cohesion c is 18.3 kPa and the internal friction angle is 28.9° , the slope stability coefficient decreases to 1. If it continues to decrease, the slope stability coefficient will be less than 1.

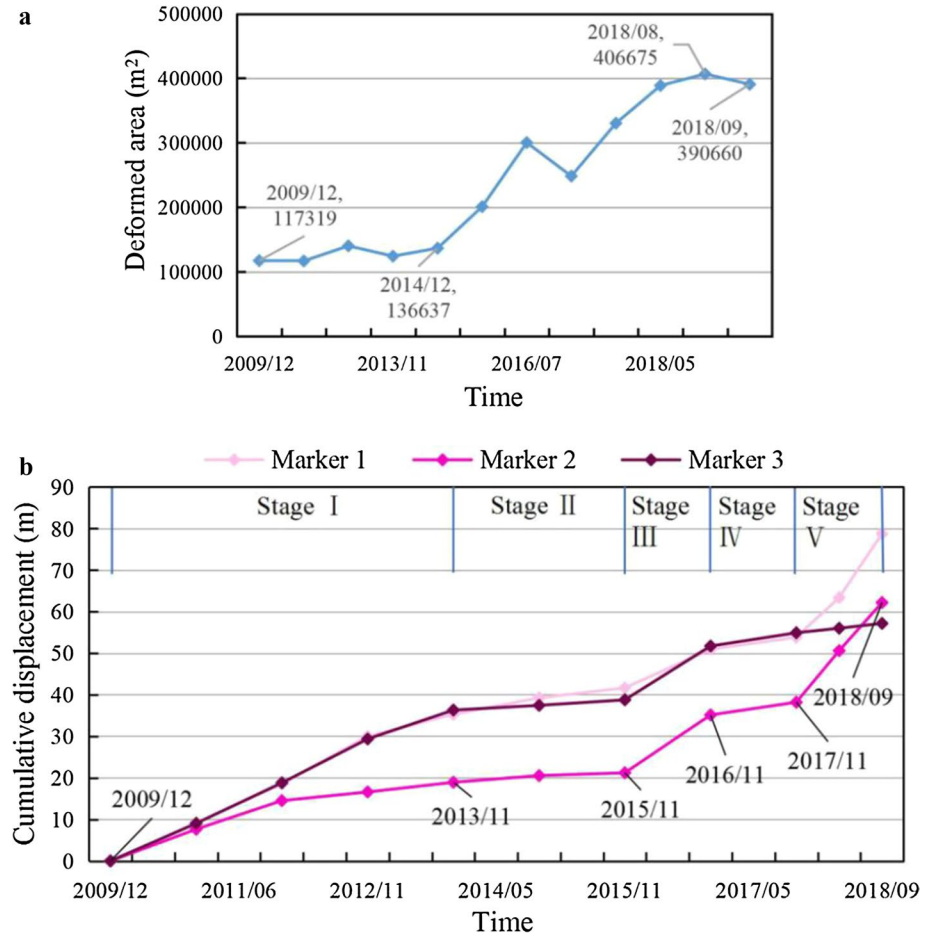


Fig. 10 Deformation process of the Baige landslide from December 2009 to August 2018. **a** The surface deformation area. **b** Cumulative displacement of the three markers

The analysis of the pre-slide slope deformation process, the rainfall, and the limit equilibrium calculation confirm that the Baige landslide was caused by gravity-induced creep.

The main body of the landslide is gneiss and greenschist in the hanging wall of the fault. It has been pushed by the hanging wall of the fault for a long time. The lower part of the landslide is granite, which is located in the foot wall of the fault and is also squeezed by the fault. The fault activity resulted in the broken rock mass and strongly weathered rock with lower strength. This kind of lithology and structure of the slope body provide good material source for the gravity-induced creep. That is, when the slope creeps to a certain extent, the shear deformation of the sliding zone becomes too large, the strength parameters are drastically reduced, the slope stability coefficient becomes less than 1.0, and a landslide occurs.

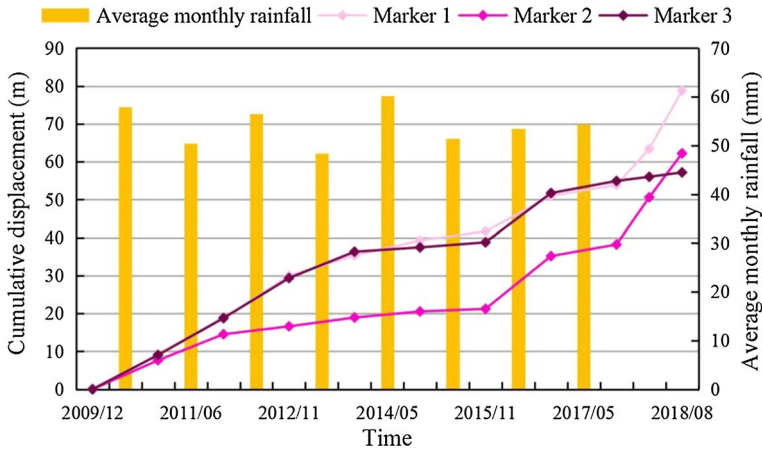


Fig. 11 Relationship between the average monthly rainfall and cumulative displacement of three markers

4.5 Future stability prediction

After the landslide, five crack-concentration zones emerged in the head scarp and either wall, named zones I–V (Fig. 13). Because the front is an exposed face with dense cracks, the stability of these zones is presumably very poor. In particular, when heavy rainfall occurred, these slopes slid very easily after the rain water entered the cracks. Based on the limit equilibrium principle, the stability coefficients of these zones were calculated using the Morgenstern-Price method. In the five crack-concentration zones, five sections were delimited for calculation (Fig. 13). From the relevant literature (Liao et al. 2013; Wang et al. 2012), the gravity γ of the slide's body was determined to be 20 g/cm^3 , the cohesion c of the slide's surface was determined to be 18.3 kPa, and the internal friction angle φ was determined to be 36.6° . The calculated stability coefficients of sections I–V are 1.256, 1.104, 1.000, 1.268, and 1.255, respectively. Although the calculation parameters were assumed, the results indicate that section C–C' in zone III, i.e., the head scarp of the landslide, has the lowest stability coefficient and the poorest stability.

5 Conclusions

In this work, two successive landsliding events which dammed the Jinsha River were presented and analyzed, including geometric characteristics, causes, and future stability. They were caused by gravity creep, not related to the rainfall. Self-weight creeping landslides generally experience long-term deformation before their total failure. The deformation process of the slope before the landsliding was inferred based on high-resolution satellite images. High-resolution images also permit to recognize large self-weight creeping landslides ahead of time. The Baige landslide caused huge losses, providing a typical example of self-weight creeping landslides in the Tibetan Plateau. The limit equilibrium calculation also indicates that the stability coefficient of the head scarp is the lowest. Thus, we suggest this place should be cut down as a priority. Further study on the exact deformation and shear strength of the soil in the head scarp should be carried out, and the stability and evolution of this region should receive more attention. This landslide also emphasizes the importance of monitoring big deformation bodies in the Tibetan Plateau, especially those on the bank slopes of big rivers.

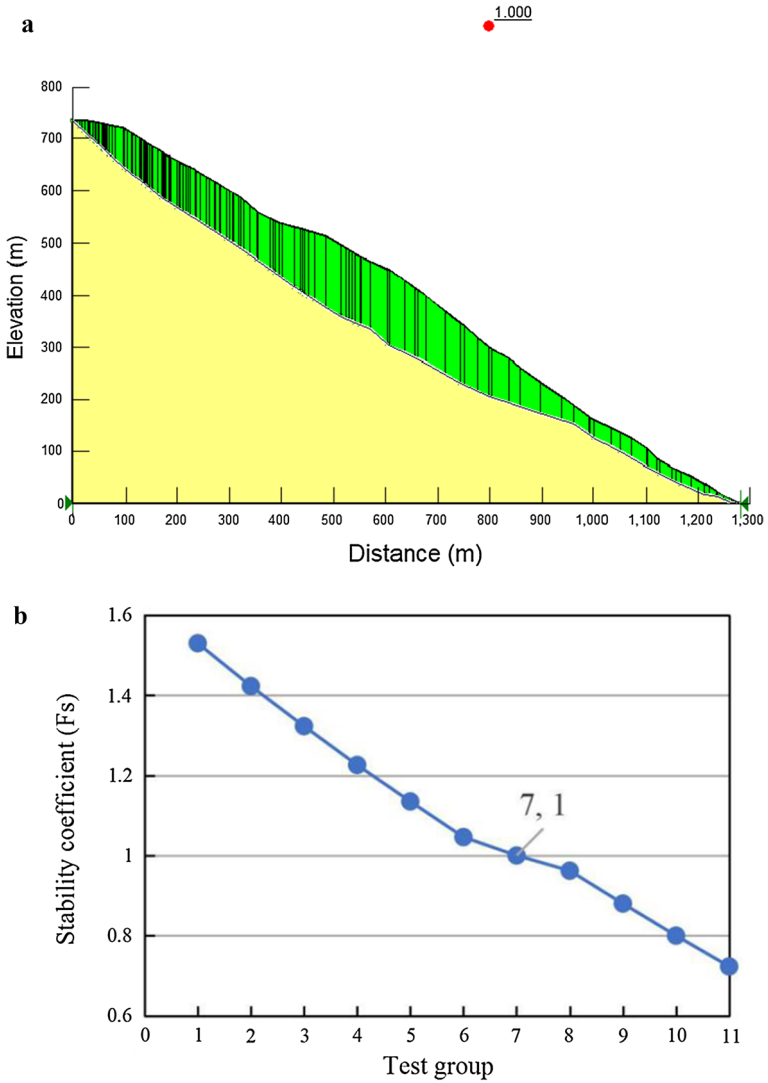
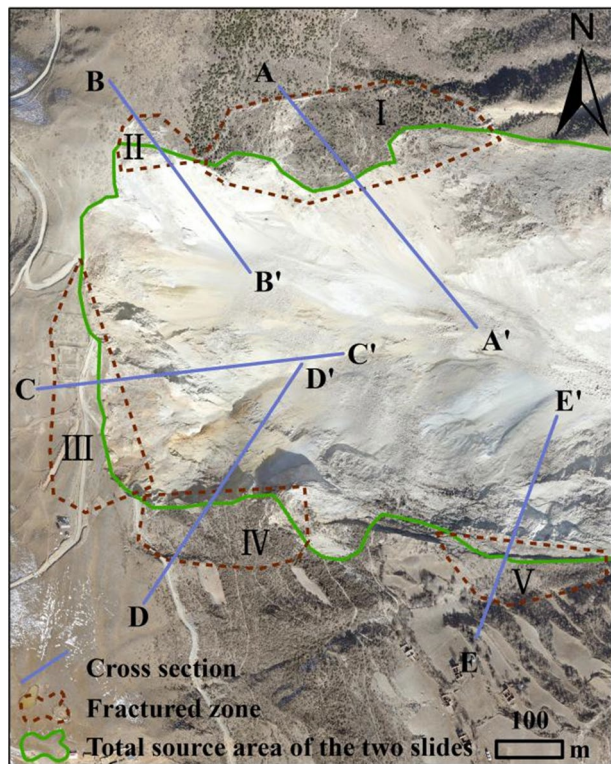


Fig. 12 Limit equilibrium calculation results for the test groups in Table 1. **a** Computational chart for $F_s = 1.0$. **b** Chart of the change in the stability coefficient

Table 1 Parameters for the limit equilibrium calculation

Test group	γ (g/cm ³)	c (kPa)	φ (°)	F_s
1	20	35	40	1.53
2	20	32	38	1.42
3	20	29	36	1.32
4	20	26	34	1.23
5	20	23	32	1.14
6	20	20	30	1.05
7	20	18.3	28.9	1
8	20	17	28	0.96
9	20	14	26	0.88
10	20	11	24	0.8
11	20	8	22	0.72

Fig. 13 The trailing edge of the Baige landslide

Acknowledgements This research was supported by the National Natural Science Foundation of China (41807267, 41661144037), the Basic Scientific and Research Fund from the National Institute of Natural Hazards, Ministry of Emergency Management of China (former Institute of Crustal Dynamics, China Earthquake Administration) (ZDJ2019-25) and the Natural Science Research Project of Colleges and Universities in Anhui Province (KJ2018A0075). We thank Ming Wen from National Institute of Natural Hazards, Ministry of Emergency Management of China, for his help in the field investigation. We also thank Dr. Thomas Glade (Editor in Chief), Dr. Sam McColl, and an anonymous reviewer for their valuable comments.

References

- Chai H, Liu H, Zhang Z (1995) The catalog of Chinese landslide dam events. *J Geol Hazard Environ Preserv* 6(4):1–9 (in Chinese)
- Chai HJ, Liu HC, Zhang ZY, Xu ZW (2000) The distribution, causes and effects of damming landslides in China. *J Chengdu Univ Technol* 27(3):302–307 (in Chinese)
- Chen J, Dai F, Lv T, Cui Z (2013) Holocene landslide-dammed lake deposits in the Upper Jinsha River, SE Tibetan Plateau and their ages. *Quatern Int* 298:107–113
- Chen J, Zhou W, Cui Z, Li W, Wu S, Ma J (2018) Formation process of a large paleolandslide-dammed lake at Xuelongnang in the upper Jinsha River, SE Tibetan Plateau: constraints from OSL and ¹⁴C dating. *Landslides* 15(12):2399–2412
- Cui Y, Xu C, Xu S, Chai S, Fu G, Bao P (2020) Small-scale catastrophic landslides in loess areas of China: an example of the March 15, 2019, Zaoiling landslide in Shanxi Province. *Landslides* 17(3):669–676
- Dai F, Lee CF, Deng J, Tham L (2005) The 1786 earthquake-triggered landslide dam and subsequent dam-break flood on the Dadu River, southwestern China. *Geomorphology* 65(3):205–221
- Deng J, Gao Y, Yu Z, Xie H (2019) Analysis on the formation mechanism and process of baige landslides damming the upper reach of Jinsha River. *China Adv Eng Sci* 51(1):9–16 (in Chinese)
- Deng Q (2007) Active Tectonic map of China. Seismogical Press, Beijing
- Evans SG, Hermanns RL, Strom A, Scarascia-Mugnozza G (2011) Natural and artificial rockslide dams, vol 133
- Fan X, Xu Q, Scaringi G, Zheng G, Huang R, Dai L, Ju Y (2019a) The “long” runout rock avalanche in Pusa, China, on August 28, 2017: a preliminary report. *Landslides* 16(1):139–154
- Fan W, Lyu J, Cao Y, Shen M, Deng L, Wei Y (2019b) Characteristics and block kinematics of a fault-related landslide in the Qinba Mountains, western China. *Eng Geol* 249:162–171
- Hu G, Liu M, Chen N, Zhang X, Wu K, Khanal BR, Han D (2019) Real-time evacuation and failure mechanism of a giant soil landslide on 19 July 2018 in Yanyuan County, Sichuan Province, China. *Landslides* 16(6):1177–1187
- Liao J, Wu Y, Ou G, Zhang Q, Cheng G (2013) Shear strength behavior of slide zone soil in ring shear tests. *J Wuhan Univ Technol* 35(10):92–95 (in Chinese)
- Long W, Chen J, Wang PF, Chong XU, Liu H, Sun JZ (2015) Formation mechanism and back analysis of paleoseismic parameters of the temi large-scale ancient landslide in the upper Jinsha River. *J Seismol Res* 37(5):71–76 (in Chinese)
- Ma S, Xu C, Shao X, Zhang P, Liang X, Tian Y (2018) Geometric and kinematic features of a landslide in Mabian Sichuan, China, derived from UAV photography. *Landslides* 16(2):373–381
- Ma S, Wei J, Xu C, Shao X, Xu S, Chai S, Cui Y (2020) UAV survey and numerical modeling of loess landslides: an example from Zaoiling, southern Shanxi Province, China. *Nat Hazards*. <https://doi.org/10.1007/s11069-020-04207-1>
- Morgenstern NR, Price VE (1965) The analysis of the stability of general slip surface. *Geotechnique* 15(1):79–93
- Ouyang C, Zhao W, An H, Zhou S, Wang D, Xu Q, Li W, Peng D (2019) Early identification and dynamic processes of ridge-top rockslides: implications from the Su Village landslide in Suichang County, Zhejiang Province, China. *Landslides* 16(4):799–813
- Varnes DJ (1958) Landslide types and processes. *Landslides Eng Pract* 24:20–47
- Wang P, Zhang B, Qiu W, Wang J (2011) Soft-sediment deformation structures from the Diexi paleo-dammed lakes in the upper reaches of the Minjiang River, east Tibet. *J Asian Earth Sci* 40(4):865–872
- Wang S, Xiang W, Cui D, Yang J, Huang X (2012) Study of residual strength of slide zone soil under different ring-shear tests. *Rock Soil Mech* 33(10):2967–2972 (in Chinese)
- Wei J, Zhao Z, Xu C, Wen Q (2019) Numerical investigation of landslide kinetics for the recent Mabian landslide (Sichuan, China). *Landslides* 16(11):2287–2298
- Wu Y, Niu R, Lu Z (2019) A fast monitor and real time early warning system for landslides in the Baige landslide damming event, Tibet, China. *Natl Hazard Earth Syst Sci*, pp 1–20
- Xu C, Xu X, Yao X, Dai F (2014) Three (nearly) complete inventories of landslides triggered by the May 12, 2008 Wenchuan Mw 7.9 earthquake of China and their spatial distribution statistical analysis. *Landslides* 11(3):441–461
- Xu C, Xu X, Shyu JBH (2015) Database and spatial distribution of landslides triggered by the Lushan, China Mw 6.6 earthquake of 20 April 2013. *Geomorphology* 248:77–92
- Xu X, Han Z, Yang X, Zhang S, Yu G, Zhou B, Li F, Ma B, Chen G, Ran Y (2016) Seismotectonic map in China and its adjacent regions. Seismogical Press, Beijing

- Yang Y-c, Xing H-g, Yang X-g, Huang K-x, Zhou J-w (2015) Two-dimensional stability analysis of a soil slope using the finite element method and the limit equilibrium principle. *IES J A: Civ Struct Eng* 8(4):251–264
- Zhang L, Xiao T, He J, Chen C (2019a) Erosion-based analysis of breaching of Baige landslide dams on the Jinsha River, China, in 2018. *Landslides* 16(10):1965–1979
- Zhang Z, He S, Liu W, Liang H, Yan S, Deng Y, Bai X, Chen Z (2019b) Source characteristics and dynamics of the October 2018 Baige landslide revealed by broadband seismograms. *Landslides* 16(4):777–785
- Zhou R, Chen G, Li Y, Zhou Z, Gong Y, He Y, Li X (2005) Research on active faults in Litang-Batang region, Western Sichuan Province, and the seismogenic structures of the 1989 Batang M67 earthquake swarm. *Seismol Geol* 27(1):31–43 (in Chinese)
- Zhou X, Cheng H (2014) Stability analysis of three-dimensional seismic landslides using the rigorous limit equilibrium method. *Eng Geol* 174:87–102
- Zhu Y, Xu S, Zhuang Y, Dai X, Xing A (2019) Analysis of characteristics and runout behaviour of the disastrous 28 August 2017 rock avalanche in Nayong, Guizhou, China. *Eng Geol* 259:1–11

Publisher's Note Springer Nature remains neutral with regard to jurisdictional claims in published maps and institutional affiliations.